



Competition of an incommensurate flux phase and superconductivity in a t - J model with Coulomb interactions

E. Cappelluti^{*}, R. Zeyher

Max-Planck-Institut für Festkörperforschung, Heisenbergstrasse 1, D-70569 Stuttgart, Germany

Received 28 August 1998; revised 10 November 1998; accepted 12 November 1998

Abstract

Based on the X -operator approach and a $1/N$ expansion, we present results for the phase diagram and in particular, the incommensurate flux phase of a generalized t - J model which also contains Coulomb interactions. It is found that the optimal T_c for superconductivity as well as the fast decrease of T_c in the underdoped regime is the result of a competition between an incommensurate flux and a superconducting phase, both having order parameters with d-wave symmetry. A charge-density wave ground state is found only at rather low dopings far away from the superconducting phase. The evolution of the single-particle gap and the associated destruction of a part of the Fermi surface are studied by means of the dispersion and density of electronic states and the optical conductivity. © 1999 Elsevier Science B.V. All rights reserved.

Keywords: Flux phase; Superconductivity; Phase diagram; Pseudogap

Many theoretical mean-field phase diagrams of the t - J model show, besides the superconducting and the normal phase, additional phases characterized by flux, charge- or spin-density wave order parameters [1–7]. Different treatments yielded quite different phase diagrams in the past. A recent X -operator approach combined with a $1/N$ expansion [7] predicted without Coulomb interactions just a d-wave superconducting phase with a transition temperature T_c which increased monotonously with decreasing doping. Turning on Coulomb interactions, most of the superconducting region at higher temperatures was replaced by a d-wave flux state. Because the two-order parameters have the same symmetry, the flux and the superconducting state compete with each other leading to a strong suppression of superconductivity in the underdoped region.

Phase diagrams based on weakly interacting slave particles [2–5] tend to give a richer variety of phases than those based on X -operators and unenlarged Hilbert spaces. This is not astonishing because many more order parameters can be formed from slave particles than from the original electrons. In Refs. [4,5], the coexistence of a flux and a d-wave resonant-valence bond state has been studied. One of the most advanced treatments using slave particles [3] predicts a flux phase atop on the superconducting phase in the underdoped region. The decrease of T_c with decreasing doping is, in this case, determined by the condensation of Bose particles which leads to a roughly linear dependence on the doping in the underdoped regime. In contrast to the X -operator

^{*} Corresponding author. Tel.: +49-711-689-1537; Fax: +49-711-689-1595; E-mail: emmcapp@audrey2.mpi-stuttgart.mpg.de

approach, phase separation and Coulomb forces do not play a role in this approach, nor can the dependence of T_c on doping be viewed as the result of a competition between the flux and the superconducting phase.

In the two approaches discussed above, it is assumed that the flux phase is commensurate with the lattice. It has, however, been shown that the flux state is commensurate only at higher temperatures, whereas it becomes incommensurate with the lattice at lower temperatures [7,8]. This observation should be relevant for the description of the competition of flux and superconducting phase. It is the purpose of this communication to generalize our previous treatment, which employed X -operators and the $1/N$ expansion, to take into account also incommensurate flux states and to describe their properties such as the density of states, the competition with superconductivity and the resulting phase diagram.

In order to study the physical properties of the incommensurate state, we first have to determine, for a given doping and temperature, the wave vectors which characterize the modulation. As previously has been discussed [9], the charge and spin response of the t - J model is determined by a 6×6 susceptibility matrix $\chi(\mathbf{q}, \omega)$. If one of the eigenvalues of $\chi(\mathbf{q}, 0)$ exceeds the value 1, the normal state is unstable towards a phase characterized by the corresponding eigenvector as order parameter and the modulation wave vector \mathbf{q} . In this way, the boundary between the normal and the new phase can be determined. Inside the new phase the largest eigenvalue of $\chi(\mathbf{q}, 0)$ will determine the modulation vector \mathbf{q} , which in general will vary throughout the phase. For a square lattice, it will be sufficient to search for \mathbf{q} within the small Brillouin zone, i.e., $1/8$ of the Brillouin zone. We find that \mathbf{q} lies, in general, along the X - M direction near the M -point (for a definition of the points X and M , see the right panel in Fig. 1). This implies that there are four inequivalent modulation vectors \mathbf{q}_i within the entire Brillouin zone given by:

$$\mathbf{q}_1 = (q_x, q_y), \quad \mathbf{q}_2 = (q_y, q_x), \quad \mathbf{q}_3 = (-q_x, -q_y), \quad \mathbf{q}_4 = (-q_y, -q_x). \quad (1)$$

It is also convenient to introduce the notation $\mathbf{q}_3 = \bar{\mathbf{q}}_1$, $\mathbf{q}_4 = \bar{\mathbf{q}}_2$.

Given the above four instability vectors, the Green's function g and the self-energy Σ satisfy the equations:

$$g(\mathbf{k}_1, \mathbf{k}_2; \omega_n) = g(\mathbf{k}_1; \omega_n) \delta(\mathbf{k}_2) N_c + \sum_i \delta g(\mathbf{k}_1, \mathbf{q}_i; \omega_n) \delta(\mathbf{k}_2 - \mathbf{q}_i) N_c, \quad (2)$$

$$\Sigma(\mathbf{k}_1, \mathbf{k}_2) = \Sigma(\mathbf{k}_1) \delta(\mathbf{k}_2) N_c + \sum_i \phi(\mathbf{k}_1, \mathbf{q}_i) \delta(\mathbf{k}_2 - \mathbf{q}_i) N_c. \quad (3)$$

Because all spin-dependent quantities are diagonal in the spin indices, we have omitted them in Eqs. (2) and (3). $g(\mathbf{k}_1, \mathbf{k}_2; \omega_n)$ and $g(\mathbf{k}_1; \omega_n)$ denote the Green's functions in the modulated and unmodulated cases, respectively. \mathbf{k}_1 and ω_n stand for the momentum and the Matsubara frequency of the electron. N_c is the number of primitive cells and $\delta(\mathbf{k})$ denotes the Kronecker symbol. The second term on the right-hand side of Eq. (2) describes the modulated part of the Green's function. Here, we have made two approximations. First, we used the plane wave limit, i.e., the momentum \mathbf{k}_2 in Eq. (2) couples only to the primary wave vectors \mathbf{q}_i but not to higher harmonics. Secondly, the modulated parts in Eqs. (2) and (3) could be general linear combinations of the

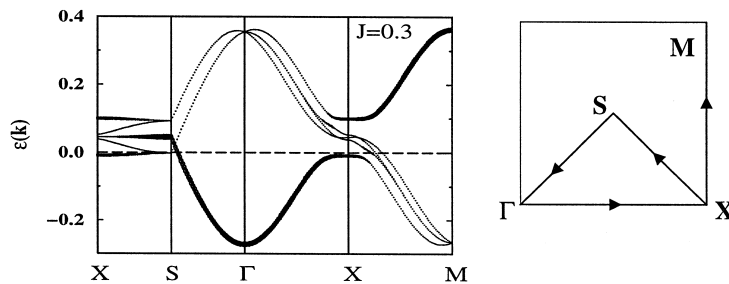


Fig. 1. Electronic dispersion in the incommensurate state at doping $\delta = 0.1$.

four waves. We have chosen the symmetric combination because this is the combination which goes over smoothly to the case of the commensurate flux phase in the limit $q_i \rightarrow (\pi, \pi)$.

The Dyson's equation for the Green's function, Eq. (2), and the self-energy, Eq. (3), can be written in the matrix form:

$$\left[i\omega_n \hat{f} - \hat{\Sigma}(\mathbf{k}, \{q_i\}) \right] \vec{g}(\mathbf{k}, \{q_i\}; \omega_n) = \vec{u}, \quad (4)$$

where

$$\vec{g}(\mathbf{k}, \{q_i\}; \omega_n) = \begin{pmatrix} g(\mathbf{k}; \omega_n) \\ \delta g(\mathbf{k} - \mathbf{q}_1, \bar{\mathbf{q}}_1; \omega_n) \\ \delta g(\mathbf{k} - \bar{\mathbf{q}}_1, \mathbf{q}_1; \omega_n) \\ \delta g(\mathbf{k} - \mathbf{q}_2, \bar{\mathbf{q}}_2; \omega_n) \\ \delta g(\mathbf{k} - \bar{\mathbf{q}}_2, \mathbf{q}_2; \omega_n) \end{pmatrix}, \quad \vec{u} = \begin{pmatrix} 1 \\ 0 \\ 0 \\ 0 \\ 0 \end{pmatrix}, \quad (5)$$

and

$$\hat{\Sigma}(\mathbf{k}, \{q_i\}) = \begin{pmatrix} \Sigma(\mathbf{k}) & \phi(\mathbf{k}, \mathbf{q}_1) & \phi(\mathbf{k}, \bar{\mathbf{q}}_1) & \phi(\mathbf{k}, \mathbf{q}_2) & \phi(\mathbf{k}, \bar{\mathbf{q}}_2) \\ \phi(\mathbf{k} - \mathbf{q}_1, \bar{\mathbf{q}}_1) & \Sigma(\mathbf{k} - \mathbf{q}_1) & 0 & 0 & 0 \\ \phi(\mathbf{k} - \bar{\mathbf{q}}_1, \mathbf{q}_1) & 0 & \Sigma(\mathbf{k} - \bar{\mathbf{q}}_1) & 0 & 0 \\ \phi(\mathbf{k} - \mathbf{q}_2, \bar{\mathbf{q}}_2) & 0 & 0 & \Sigma(\mathbf{k} - \mathbf{q}_2) & 0 \\ \phi(\mathbf{k} - \bar{\mathbf{q}}_2, \mathbf{q}_2) & 0 & 0 & 0 & \Sigma(\mathbf{k} - \bar{\mathbf{q}}_2) \end{pmatrix}. \quad (6)$$

It can be seen that $\phi(\mathbf{k} - \mathbf{q}_i, \bar{\mathbf{q}}_i) = \phi(\mathbf{k} - \bar{\mathbf{q}}_i, \mathbf{q}_i)$, so that the excitation spectrum is real. Finally, the matrix elements of the self-energy in Eq. (6) have to be calculated explicitly in terms of g , similar as in Ref. [7]. After this step, Eqs. (4)–(6) are closed.

Assuming that the order parameters ϕ are small, Eqs. (4)–(6) can be linearized in ϕ and reduce then to the equations investigated in Ref. [7]. In order to be able to discuss the incommensurate phase also far away from its boundaries, we have solved the nonlinear Eqs. (4)–(6) by numerical means. The obtained electronic dispersion along the high-symmetry axes X – S – Γ – X – M [$X = (\pi, 0)$, $S = (\pi/2, \pi/2)$, $\Gamma = (0, 0)$, $M = (\pi, \pi)$] is shown in Fig. 1 for the doping $\delta = 0.1$ and for zero temperature. The position of the various points in the Brillouin zone are explained in the panel at the right-hand side. The thickness of the lines is proportional to the spectral weight of the corresponding branch in the diagonal Green's function $g(\mathbf{k}, \omega_n)$. The band energies are given relative to the chemical potential. Here and in the following, all energies are given in units of t . A typical value for t is 0.3 eV for high- T_c compounds. In the normal state, for instance at high temperatures, there is only one band given essentially by the thickest line in Fig. 1, but without a gap at X and without dispersion along the X – S direction. Lowering the temperature, we reach the commensurate phase with an order parameter $\phi(\mathbf{k}, Q_c) \sim i[\cos(k_x) - \cos(k_y)]$ with $Q_c = (\pi, \pi)$ and two bands. Electrons near the X -point interact strongly with those near the point $Y = (0, \pi)$ creating a gap between the two bands at the X -point. Electrons at the S -point are unperturbed so the two bands are degenerate at the point S . Along the directions S – X , the two bands split to form the gap at the point X . At still lower temperatures q_y moves away from π in an essentially linear manner towards smaller values. At very low temperatures and $\delta = 0.1$, it has decreased by about 10%. There are now five electronic bands in Fig. 1. The gap at the X -point is essentially unchanged but it hosts three unoccupied in-gap bands. At the S -point, the band of the high temperature normal phase splits into a strong, unshifted central component and two twofold degenerate bands lying symmetrically at higher and lower energies. As a result, we obtain three very flat bands with rapidly changing spectral weight in the direction S – X , one of them is partly occupied.

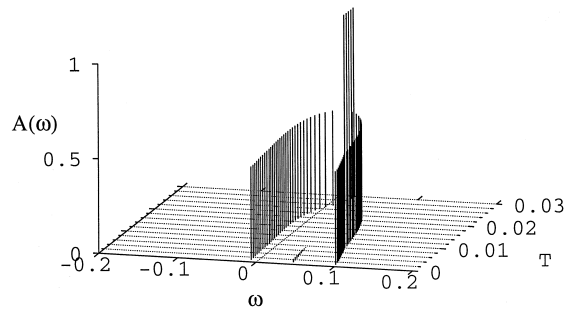


Fig. 2. Spectral function for several temperatures and $J = 0.3$ at doping $\delta = 0.1$.

The evolution of the spectral function $A(\omega)$ of the Green's function $g(\mathbf{k}, \omega)$ at the X -point with temperature T is shown in Fig. 2. The height of the vertical lines indicates the spectral weight in each delta function and the doping value is 0.1. For $T < 0.01$, the system is in the incommensurate flux state. The spectral weight is mainly in the two bands forming the gap whereas there is only little weight in the three in-gap bands. For $T/t > \sim 0.0087$, the system becomes commensurate and reaches the normal state at $T/t > \sim 0.03$.

Figs. 1 and 2 clearly demonstrate that the normal state instability towards a flux state is a strong instability. The resulting gap in the one-particle spectrum is about $0.1t$ at low temperatures and thus, about $1/5$ of the band width at $\delta = 0.1$. Another feature of Figs. 1 and 2 is that the one-particle gap at the X -point lies symmetrically with respect to the chemical potential at half-filling but very unsymmetrical with respect to the actual chemical potential. This is quite in contrast to the Peierls instability in one dimension. In our case, the large van Hove singularity at half-filling, two-dimensional effects and the d -wave symmetry of the order parameter play an important role. Remarkable are, in our case, the flat bands in the direction X - S which create large density of state peaks near the Fermi energy.

The density of states at zero temperature is shown in Fig. 3 for dopings $\delta = 0.02, 0.04, \dots, 0.16$. The upper panel at the left corresponds to the lowest, the lower panel at the right to the highest doping. First, we note that the band width increases strongly with doping. At zero doping, it is determined by J but increases with increasing doping more and more because the larger hopping energy t becomes the dominating energy scale. The transition from the incommensurate flux to the normal state occurs at $\delta \sim 0.14$. At the smallest doping value, we see a large d -wave gap in the density of states which lies rather symmetrically to the chemical potential and is larger than half of the whole band width. With increasing doping up to about $\delta \sim 0.1$, the

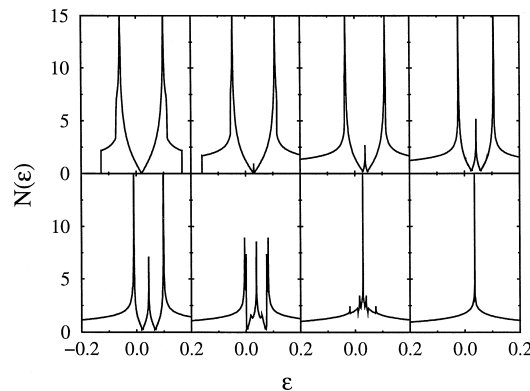


Fig. 3. Density of state for $J = 0.3$ and different dopings $\delta = 0.02, 0.04, \dots, 0.16$.

d-wave gap does not change much. However, the chemical position moves more and more to the lower edge of the gap making the system more and more metallic. At the same time, unoccupied midgap states appear with increasing spectral weight. They are due to the flat band in direction X – S which lies near the chemical position of the half-filled case, i.e., in the middle of the gap. They are unshifted because of the d-wave symmetry of the order parameter. The gap shrinks above $\delta = 0.10$ and closes around $\delta = 0.14$. The panels in Fig. 3 exhibit many extremely sharp peaks. In the normal state for $\delta = 0.16$, the density peak is due to the van Hove singularity. At lower dopings, the edge peaks of the gap can be approximately considered as van Hove peaks at the X -point which are additionally sharpened up by the weak dispersion between the X and the S points. The virtual absence of dispersion along the direction X – S of the band in the middle in Fig. 1 pins the midgap states to the center of the gap producing there a sharp peak.

The evolution of the Fermi surface with doping is shown in Fig. 4. In the extreme cases of zero doping and $\delta = 0.16$, the Fermi surface consists of one point at the S -point and the usual Γ -centered continuous line in the normal state, respectively. For dopings between these extreme cases, we have defined the Fermi surface as the set of all \mathbf{k} -points with energies equal to the Fermi energy and a spectral weight larger than 0.1 in the diagonal Green's function $g(\mathbf{k}, \omega)$. With increasing doping, a hole pocket forms around the point S which extends more and more along the line S – X . Beyond $\delta = 0.10$, separate pieces around the X -point appear which then grow together to form finally the Fermi line of the normal state. Available photoemission data [11] are presently not detailed enough for a quantitative comparison with Fig. 4 but there is at least qualitative agreement.

Having obtained the Green's function, we can also calculate the optical conductivity $\sigma(\omega)$. Generalizing the Mattis–Bardeen theory [10] to the incommensurate phase the real part of the in-plane optical conductivity is given by:

$$\sigma(\omega) \sim -\frac{1}{N_c^2} \sum_{\mathbf{k}, \mathbf{k}'} \int_{-\infty}^{\infty} \frac{dz}{\pi} f(z) \text{Im} \vec{g}_R(\mathbf{k}, \{\mathbf{q}_i\}; z) \cdot [\text{Im} \vec{g}_R(\mathbf{k}', \{\mathbf{q}_i\}; z + \omega) - \text{Im} \vec{g}_R(\mathbf{k}', \{\mathbf{q}_i\}; z - \omega)]. \quad (7)$$

\vec{g}_R denotes the analytically continued Green's function vector \vec{g} defined in Eq. (4) using retarded boundary conditions. f denotes the Fermi function. Fig. 5 shows the calculated optical conductivity for three different temperatures $T = 0.0, 1.92 \times 10^{-2},$ and 2.56×10^{-2} . The peak at the highest frequency corresponds for all temperatures to transitions near the X -point across the pseudogap. The pseudogap shrinks at higher temperatures which shifts this highest peak towards lower frequencies. Each curve exhibits a Drude peak at $\omega \sim 0$ due to transitions near the pieces of the Fermi line left over after the formation of the gap. The zero-temperature curve

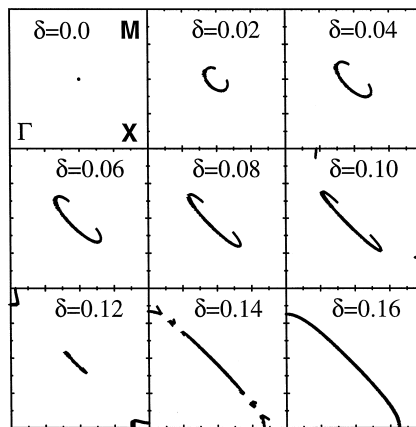


Fig. 4. Evolution of the Fermi surface with doping for $J = 0.3$.

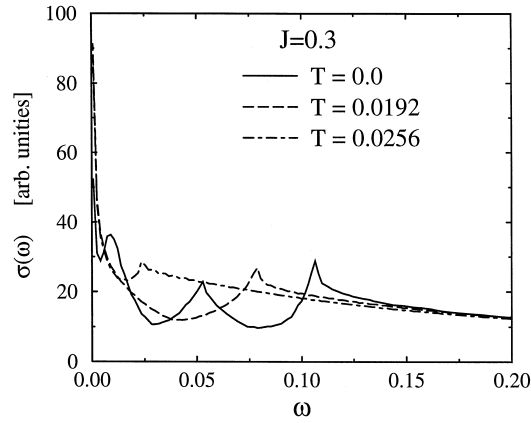


Fig. 5. Optical conductivity in the Mattis–Bardeen approximation for $\delta = 0.1$ and the temperatures $T = 0.0, 1.92 \times 10^{-2}$, and 2.56×10^{-2} .

in Fig. 5 shows additional structures. One peak lies halfway to the upper peak and is caused by transitions to the unoccupied midgap states, mainly around the S -point. There is another peak-like structure at rather low frequencies due to transitions from occupied states near the chemical potential to the midgap states. The essential features of Fig. 5 (narrowing of the Drude peak and loss of spectral weight above the Drude peak) are in agreement with experimental spectra [12].

Finally, the instability towards the superconducting phase can be studied by allowing anomalous parts in the self-energy and the Green's function, which will be denoted by $\hat{\Sigma}^{\sigma\bar{\sigma}}(\mathbf{k}, \{\mathbf{q}_i\})$ and $\vec{g}^{\sigma\bar{\sigma}}(\mathbf{k}, \{\mathbf{q}_i\}; \omega_n)$, respectively. We consider singlet pairing so that the explicitly shown spin indices have the form $\sigma\bar{\sigma}$ where $\bar{\sigma}$ denotes the opposite spin direction of σ . Note also that the superconducting order parameter does not interfere with the translational symmetry of the normal state. As a result, only the first component $g_1^{\sigma\bar{\sigma}}(\mathbf{k}, \{\mathbf{q}_i\}; \omega_n) = g^{\sigma\bar{\sigma}}(\mathbf{k}; \omega_n)$ of the anomalous Green's function is nonzero and the matrix $\hat{\Sigma}^{\sigma\bar{\sigma}}$ is diagonal:

$$\hat{\Sigma}^{\sigma\bar{\sigma}}(\mathbf{k}, \{\mathbf{q}_i\}) = \begin{pmatrix} \Sigma^{\sigma\bar{\sigma}}(\mathbf{k}) & 0 & 0 & 0 & 0 \\ 0 & \Sigma^{\sigma\bar{\sigma}}(\mathbf{k} - \mathbf{q}_1) & 0 & 0 & 0 \\ 0 & 0 & \Sigma^{\sigma\bar{\sigma}}(\mathbf{k} - \mathbf{q}_1) & 0 & 0 \\ 0 & 0 & 0 & \Sigma^{\sigma\bar{\sigma}}(\mathbf{k} - \mathbf{q}_2) & 0 \\ 0 & 0 & 0 & 0 & \Sigma^{\sigma\bar{\sigma}}(\mathbf{k} - \mathbf{q}_2) \end{pmatrix}. \quad (8)$$

For our purposes, it is sufficient to linearize Dyson's equation which yields:

$$g^{\sigma\bar{\sigma}}(\mathbf{k}; \omega_n) = \sum_{\alpha} g_{\alpha}^{\sigma\sigma}(\mathbf{k}, \{\mathbf{q}_i\}) \Sigma_{\alpha\alpha}^{\sigma\bar{\sigma}}(\mathbf{k}, \{\mathbf{q}_i\}) g_{\alpha}^{\bar{\sigma}\bar{\sigma}}(\mathbf{k}, \{\mathbf{q}_i\}). \quad (9)$$

The anomalous self-energy $\Sigma_{\alpha\alpha}^{\sigma\bar{\sigma}}(\mathbf{k}, \{\mathbf{q}_i\})$ is coupled back to the Green's function via the mean-field expression:

$$\Sigma^{\sigma\bar{\sigma}}(\mathbf{k}) = -\frac{1}{2N_c} \sum_p [J(\mathbf{k} + \mathbf{p}) - V_d(\mathbf{k} + \mathbf{p})] T \sum_n g^{\sigma\bar{\sigma}}(\mathbf{p}; \omega_n) e^{i\omega_n 0^+}, \quad (10)$$

where $V_d(\mathbf{k})$ is the screened Coulomb interaction projected onto the d-wave symmetry. The transition line between the incommensurate and the superconducting phase can be calculated from Eqs. (9) and (10) by demanding that these homogenous equations develop a non-vanishing solution at the boundary. Moreover, we will confine ourselves to d-wave superconductivity because this symmetry has the highest transition temperature in our model.

Disregarding Coulomb interactions, the calculated phase diagram contains only the normal and the superconducting phase with a T_c monotonously increasing with decreasing doping δ . Qualitatively, the T_c -line interpolates smoothly between the solid line in Fig. 6 for $\delta > 0.15$, shifted upwards by roughly a factor 2, and the upper solid line for $\delta < 0.15$. The upper solid line reaches a maximum for $\delta \rightarrow 0$ making there the superconducting state equivalent with a resonant valence bond state due to the additional SU(2) symmetry at this point. The transition to this resonance valence bond state occurs already at a rather large temperature which makes plausible that the curve for T_c has to exhibit a maximum at zero doping. Things change dramatically if the Coulomb potential V_d is also included. We have used the parameters of Ref. [13] for V_d and scaled in addition V_d such that its nearest-neighbor part V_{nn} is equal to $J/2$. The solid and dashed lines show the result for $V_{nn} = J/2$. Disregarding superconductivity first, there appears a quantum critical point at $T = 0$ and $\delta = \delta_c \sim 0.14$ which separates the normal state at high dopings from an incommensurate flux state at low dopings. The steeply rising solid line starting from the quantum critical point separates the normal state (N) on the right from an incommensurate flux state (IFL) below the dashed line and a commensurate flux state (CFL) above the dashed line on the left. Allowing now also for superconductivity, the T_c curve is somewhat suppressed for $\delta > \delta_c$ compared to the case $V_{nn} = 0$. A much stronger T_c suppression occurs, however, on the underdoped side $\delta < \delta_c$. Here, the flux phase and the superconducting phase, having order parameters of the same symmetry, compete with each other. Since the flux instability is much stronger than the superconducting instability, the flux phase suppresses heavily the superconducting phase. The result is an optimal T_c tight to the onset of the flux instability at around δ_c and a strongly decreasing T_c with decreasing doping. The dotted line in Fig. 6 is the instability line for the formation of an incommensurate charge-density wave (ICDW). At lower temperatures, it is confined to small dopings and thus of little importance for the superconducting phase and the optimal T_c .

In conclusion, we have shown that Coulomb forces have a profound influence on the mean-field diagram of the t - J model. Disregarding them, the phase diagram possesses only a normal and a superconducting phase. Including them stabilizes the inherent flux phase in the underdoped regime. The optimal T_c as well the rapid suppression of T_c towards small dopings is the result of a competition of an incommensurate flux phase with d-wave symmetry and the superconducting phase. An incommensurate charge-density wave state is also produced by the Coulomb forces but far away from the superconducting phase and is thus of less interest. We propose that a similar quantum critical point scenario as in Refs. [1,6] is applicable with the role of antiferromagnetism or charge-density waves played by the incommensurate flux phase. Comparing with our previous treatment where the flux phase was assumed to be commensurate [7], one notes that the incommensura-

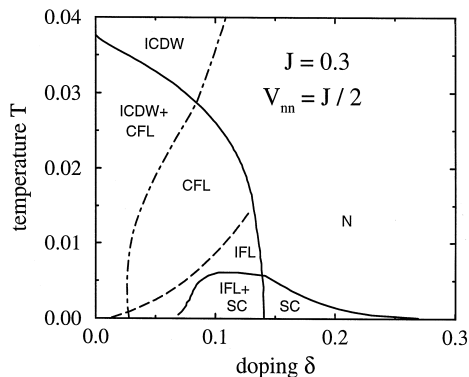


Fig. 6. Phase diagram of the t - J model with Coulomb forces. N, SC, CFL, IFL, ICDW denote the normal, superconducting, commensurate flux, incommensurate flux and incommensurate charge-density wave states, respectively.

bility of the flux phase at lower temperatures does not play a decisive role in the phase diagram. However, many features of the electronic excitation spectrum such as the existence of midgap states, the density of states or the details of the destruction of the Fermi surface by the gap depend on the incommensurability of the flux phase.

References

- [1] V. Barzykin, D. Pines, *Phys. Rev. B* 52 (1995) 13585.
- [2] X.G. Wen, P.A. Lee, *Phys. Rev. Lett.* 76 (1996) 503.
- [3] P.A. Lee, X.G. Wen, *Phys. Rev. Lett.* 78 (1997) 4111.
- [4] X. Dai, Z.-B. Su, L. Yu, *Phys. Rev. B* 56 (1997) 5583.
- [5] P.A. Marchetti, Z.-B. Su, L. Yu, *Phys. Rev. B* 58 (1998) 5808.
- [6] C. Castellani, C. Di Castro, M. Grilli, *Z. Phys. B* 103 (1997) 137.
- [7] E. Cappelluti, R. Zeyher, *cond-mat/9808201*.
- [8] D.C. Morse, T. Lubensky, *Phys. Rev. B* 42 (1990) 7794.
- [9] R. Zeyher, M. Kulić, *Phys. Rev. B* 54 (1996) 8985.
- [10] G.D. Mahan, *Many-Particle Physics*, Plenum, New York, 1990.
- [11] M.R. Norman, H. Ding, M. Randeira, J.C. Campuzano, T. Yokoya, T. Takeuchi, T. Takahashi, T. Mochiku, K. Kadowaki, P. Guptasarma, D.G. Hinks, *Nature* 392 (1998) 157.
- [12] D.N. Basov, R. Liang, B. Dabrowski, D.A. Bonn, W.N. Hardy, T. Timusk, *Phys. Rev. Lett.* 77 (1996) 4090.
- [13] F. Becca, M. Tarquini, M. Grilli, C. Castellani, *Phys. Rev. B* 54 (1996) 12443.